HETEROTOPIC BONE FORMATION BY NANO-APATITE CONTAINING POLY(D,L-LACTIDE) COMPOSITES

D. Barbieri[1*], A.J.S. Renard[2], J.D. de Bruijn[1,3], and H. Yuan[1,4]

[1] Xpand Biotechnology BV, 3723 MB Bilthoven, the Netherlands
[2] Orthopaedics Department, Medisch Spectrum Twente, 7500 KA Enschede, the Netherlands
[3] Department of Materials, Queen Mary University of London, London, E1 4NS, UK
[4] Tissue Regeneration, University of Twente, 7522 NB Enschede, the Netherlands

Abstract

To render polymeric materials osteoinductive, nano-sized calcium phosphate apatite particles (CaP) were introduced into a low molecular weight poly(D,L-lactide). Homogenous composites were made with 10%, 20% and 40% by weight of apatite content while pure polylactide was used as control. Thereafter porous samples (pore size 300-400 μm, 60% porosity) were fabricated and sterilized. *In vitro* studies showed that calcium ions were released from the composites depending on the apatite content, while surface mineral deposition was observed only on the 40% CaP composites in simulated body fluid (SBF) within 14 days. After 12 weeks of intramuscular implantation in dogs, only the 40% CaP composite implant retained its shape and showed ectopic bone formation within the pores. In conclusion, adding a content of 40% apatite into poly(D,L-lactide) could lead to an osteoinductive material. Future studies will focus on understanding this phenomenon of material-directed osteoinduction in order to develop a promising bone graft substitute.

Keywords: Osteoinduction, nano-apatite, poly(D,L-lactide), graft substitute

*Address for correspondence:
D. Barbieri
Xpand Biotechnology BV
3723 MB Bilthoven, the Netherlands
Telephone Number: +31 30 229 7280
FAX Number: +31 30 229 7299
E-mail: davide.barbieri@progentix.com

Introduction

Current methods to treat lost or damaged bone include the use of autograft and (processed) allograft. Autograft is considered the gold standard for bone repair but may lead to donor-site morbidity and has limited availability. Allograft does not have these complications but has the risk of disease transfer, immunogenicity and reduced osteoinduction (Giannoudis *et al*., 2005). An alternative to these natural bone grafts is the use of synthetic materials that ideally should be non-toxic, resorbable, osteoconductive, osteoinductive and have mechanical properties to suit their clinical application. Osteoinduction can be introduced in materials by the addition of osteogenic cells or growth factors such as rhBMP2, although some materials have been reported to have 'intrinsic' osteoinductive properties by virtue of their physicochemical characteristics (Yamasaki, 1990; Ripamonti, 1996; Yuan *et al*., 1998; Ripamonti *et al*., 1999; Yuan *et al*., 1999; Habibovic *et al*., 2005; Le Nihouannen *et al*., 2005; Kondo *et al*., 2006; de Bruijn *et al*., 2008; Fellah *et al*., 2008). Osteoinduction can be determined by the ability of a material to induce bone formation after implantation in non-osseous or ectopic sites. Winter and Simpson (1969) were the first to report on ectopic bone formation by polyHEMA. This was later followed by reports showing similar phenomena with titanium (Fujibayashi *et al*., 2004) and calcium phosphate ceramics (Yamasaki, 1990; Ripamonti, 1996; Yuan *et al*., 1998; Ripamonti *et al*., 1999; Yuan *et al*., 1999; Habibovic *et al*., 2005; Le Nihouannen *et al*., 2005; Kondo *et al*., 2006; de Bruijn *et al*., 2008; Fellah *et al*., 2008). With the latter, evidence has been provided showing that physicochemistry and surface microstructure play a role in the bone inductive potential of these materials. Examples of such osteoinductive calcium phosphate ceramics are hydroxyapatite (HA), biphasic calcium phosphate (BCP) and tricalcium phosphate (TCP) (Yamasaki, 1990; Ripamonti, 1996; Yuan *et al*., 1998; Ripamonti *et al*., 1999; Yuan *et al*., 1999; Habibovic *et al*., 2005; Le Nihouannen *et al*., 2005; Kondo *et al*., 2006; de Bruijn *et al*., 2008; Fellah *et al*., 2008). In the past years, it has been demonstrated that osteoinductive calcium phosphate ceramics can provide fast bone repair and allow effective healing of critical-sized bone defects (Kruyt *et al*., 2004; Habibovic *et al*., 2006a). The inherent brittleness of these materials however still limits their application in load-bearing sites, indicating a role for mechanically stronger materials such as osteoinductive composites.

Polymers (e.g., polyesters, polyphosphazenes, polyanhydrides and polyorthoesters) have been used as

implants for many medical applications (Rezwan *et al.*, 2006; Navarro *et al.*, 2008). Amongst the synthetic biodegradable polyesters, polylactic acid is biocompatible and resorbs within a few years into non-toxic components that can be cleared from the body. Polylactide has been approved by the US Food and Drug Administration for medical purposes and has been used in screws, sutures, scaffolds for tissue engineering and drug delivery applications. It has adequate mechanical properties for certain applications (e.g. screws and plates), but it is too elastic and therefore not suitable as a load-bearing bone replacement material (Rezwan *et al*., 2006). Attention has been paid on introducing calcium phosphates into polylactide to improve the mechanical properties and biological performance (e.g. osteoconductivity). Several of these studies have shown that adding (micro or nano) hydroxyapatite particulate or fibres into polylactide materials can improve the mechanical properties of the material (Deng *et al.*, 2001; Nejati *et al*., 2008). In addition, it was reported that the addition of more than 40 wt% hydroxyapatite can render the material osteoconductive (Verheyen, 1993). The presence of hydroxyapatite crystals has further shown to increase protein adsorption and enhance osteoblast adhesion (Verheyen, 1993; Wei and Ma, 2004; Lin *et al*., 2007). Thus far, however, none of these composites has shown to be osteoinductive.

In this study we present an approach to produce nano-apatite/polylactide composites by introducing different amounts of nano-sized apatite into poly(D,L-lactide). We evaluated the materials both *in vitro* and *in vivo* regarding their chemistry, ion release rate, surface mineralisation and osteoinductivity and hypothesize that adding increasing amounts of nano-apatite to a polymer will generate a specific surface microstructure that results in an osteoinductive composite. More apatite particles exposed at the surface will allow higher ion release, protein adsorption and surface mineralization that should further enhance the bone regenerative properties (Yuan *et al*., 1999; Habibovic *et al*., 2006b).

Materials and Methods

Nano-apatite synthesis and characterization

Nano-apatite was prepared using a wet-precipitation reaction (Rodríguez-Lorenzo and Vallet-Regí, 2000): $(NH_4)_2HPO_4$ (Fluka, Steinheim, Germany) aqueous solution (concentration 63.12 g/l) was added to $Ca(NO_3)_2 \cdot 4H_2O$ (Fluka) aqueous solution (concentration 117.5 g/l) with controlled speed (12.5 ml/min) at 80±5ºC. The reaction pH was kept above 10 by using ammonia (Fluka) as a buffer. After precipitation, the resulting apatite powder was aged overnight, washed using distilled water to remove ammonia and finally suspended in acetone (Fluka) at a concentration of 0.112±0.004 g/ml. A small amount of the powder was then sintered at 1100°C for 200 min (Nabertherm C19, Nabertherm, Lilienthal, Germany) for chemical characterization. Both the non-sintered and sintered apatite was characterized by using Fourier transform infrared spectrometer (FTIR, Perkin Elmer Spectrum 1000, Perkin Elmer, Waltham, MA, USA) and X-ray diffractometer (XRD, Rigaku MiniFlex I, Rigaku, Tokyo, Japan). The particle size and morphology of the non-sintered apatite was characterized by environmental scanning electron microscopy (ESEM, Philips XL 30 ESEM-FEG, Philips, Eindhoven, the Netherlands) in the secondary electron mode.

Preparation and characterisation of nano-apatite / poly(D,L-lactide) composites

Poly(D,L-lactide) with M_w=52,000 (Phusis Matériaux Biorésorbables, Saint Ismier, France) was dissolved in acetone (concentration 0.33 g/ml) and used to prepare four materials with different contents of non-sintered apatite: 0%, 10%, 20% and 40% by weight (0% CaP, 10% CaP, 20% CaP and 40% CaP respectively). The suspension of apatite in acetone and the polylactide solution was blended for four hours through a rotational ball milling system using glass beads (diameter 3-10 mm, total beads volume about 1/3 of the milling room volume) at room temperature and rotational speed of 12 rpm. Five ml of each mixture (3 samples per mixture) were collected and the density of the composites was determined using the weight/volume method (Archimedes principle) after complete evaporation of acetone from the samples. Sodium chloride granules with a size range of 300-400 μm (NaCl, Fluka) were added to the mixtures (60% in volume) and uniformly mixed in order to obtain porous blocks. After evaporation of the acetone and leaching of the NaCl granules with distilled water, porous bodies were obtained (pore size 300-400 μm, 60% porosity). Regular shaped porous blocks (dimension 7×7×7 mm) and irregularly shaped granules (dimension 2-3 mm) were manufactured and sterilized by γ-irradiation (irradiation dose range 28.9-30.7 kGy, IsoTron Nederland BV, Ede, the Netherlands) for further studies. The chemistry of the composites was analyzed with FTIR, and the surface morphology and apatite distribution in the polymer matrix was observed with scanning electron microscopy (SEM) (secondary electron and backscattered electron modes respectively).

In vitro calcium ion release

A simulated physiological solution (SPS) was prepared by dissolving NaCl (Merck, Darmstadt, Germany; concentration 8.00 g/l) and 4-(2-hydroxyethyl)-1-piperazineethane-sulfonic acid (HEPES) (Sigma-Aldrich, Steinheim, Germany; concentration 11.92 g/l) in distilled water. The pH of the solution was adjusted to 7.3 with 2M NaOH (Sigma-Aldrich). Calcium ion release was evaluated by soaking the irregularly shaped composite granules (2-3 mm, volume 0.13±0.005 cc) in 100 ml of SPS at 37±1°C for eight hours. While stirring at 150±5 rpm using a stirring bar (L=24 mm; ∅=6 mm), the calcium ion concentration in SPS was recorded each minute using a calcium electrode (Metrohm 692 ISE meter, Ag/AgCl reference electrode, Metrohm, Herisau, Switzerland).

In vitro surface mineralization

Simulated body fluid (SBF) was prepared according to Kokubo (Kokubo and Takadama, 2006) by dissolving reagent grade chemicals (Merck) in distilled water in strictly the following order: NaCl, $NaHCO_3$, KCl,

$K_2HPO_4 \cdot 3H_20$, $MgCl_2 \cdot 6H_2O$, $CaCl_2$ (Ca ion standard solution (0.1M), Metrohm) and Na_2SO_4. The fluid was then buffered to pH 7.4 at 36.5°C using Tris ($(CH_2OH)_3CNH_3$) and 1M HCl. The final solution had an ion concentration (in mM) as follows: Na^+, 142; K^+, 5; Mg^{2+}, 1.5; Ca^{2+}, 2.5; Cl^-, 147.8; $(HCO_3)^-$, 4.2; $(HPO_4)^{2-}$, 1; $(SO_4)^{2-}$, 0.5. Porous granules of the composites (n=20 per material, 2-3 mm) were soaked in 200 ml of SBF at 37±1°C for 2 weeks. The SBF was refreshed after 4 and 7 days. After 1, 2, 4, 7 and 14 days a minimum of 3 granules were taken out, rinsed minimal five times with distilled water, dried at room temperature, gold sputtered and observed with ESEM.

Animal experiments

With the permission of the local animal care committee (Animal Center, Sichuan University, Chengdu, China; protocol # P07015), porous blocks (7×7×7 mm, n=7 per material) were implanted in the paraspinal muscles of 7 skeletally mature mongrel dogs (male, 1-4 years old, weight 10-15 kg) for 12 weeks to evaluate the tissue reaction and osteoinductive property of the composites. The surgical procedure was performed under general anaesthesia (pentobarbital sodium, Organon, now Merck, Whitehouse Station, NJ, USA; 30 mg/kg body weight) and sterile conditions. The back of the dogs was shaved and the skin was cleaned with iodine. A longitudinal incision was made and the paraspinal muscle was exposed by blunt separation. Longitudinal muscle incisions were subsequently made with a scalpel and four separate muscle pouches were created by blunt separation (two pouches per side). The composite blocks were then placed in the pouches and the wound was closed in layers using silk sutures. After surgery, the animals received an intramuscular injection of penicillin for 3 consecutive days to prevent infection. Calcein (Sigma, St. Louis, MO, USA; 2 mg/kg body weight), xylenol orange (Sigma; 50 mg/kg body weight) and tetracycline (Sigma; 20 mg/kg body weight) were intravenously injected 3, 6 and 9 weeks after the implantation respectively to monitor the onset and time course of bone formation.

Twelve weeks after implantation, the animals were sacrificed and the samples were harvested with surrounding tissues and fixed in 4% buffered formaldehyde solution (pH=7.4) at 4°C for one week. After rinsing with phosphate buffer solution (PBS), the samples were trimmed from surrounding soft tissues, dehydrated in a series of ethanol solutions (70%, 80%, 90%, 95% and 100% ×2), and embedded in methyl methacrylate (MMA, LTI Nederland, Bilthoven, the Netherlands). Non-decalcified histological sections (10-20 μm thick) were made using a diamond saw microtome (Leica SP1600, Leica Microsystems, Wetzlar, Germany). Sections for light microscopic observations were stained with 1% methylene blue (Aldrich) and 0.3% basic fuchsin (Aldrich) solutions, while unstained sections were prepared for fluorescent microscope observations.

Histological and histomorphometric analysis

The stained sections were scanned using a slide scanner (Dimage Scan Elite 5400II, Konica Minolta Photo Imaging Inc, Tokyo, Japan) to obtain low magnification images for histomorphometric analysis. The sections were observed with a light microscope (Nikon Eclipse E200, Tokyo, Japan) to analyse the tissue reaction and bone formation. Unstained sections were observed with a fluorescent microscope (Nikon Eclipse E600, camera Nikon FDX-35) to determine the onset of bone formation.

Histomorphometry was performed using Adobe Photoshop Elements 4.0 software. Firstly the whole sample was selected as a region of interest and the corresponding number of pixels was read as *ROI*. Then the material and mineralized bone were pseudo-coloured, and their respective pixels were counted as *M* and *B* respectively. The percentage of bone in the available space of the explants (B_p%) was determined as:

$$B_p\% = \frac{B * 100}{ROI - M} \quad (1)$$

Statistical analysis

One tail paired *t*-test was used to evaluate the differences between the data and a *p*-value lower than 0.05 was considered as a significant difference. Statistical analysis was performed by using Microsoft Excel 2003 for the data elaboration and SPSS (Chicago, IL, USA) 11.5 for *t*-test.

Results

Materials characterization

Nano-apatite. FTIR spectra showed that the non-sintered apatite had similar chemistry to the sintered apatite, as indicated by the presence of all the characteristic peaks of hydroxyapatite (Fig. 1a). The XRD pattern of sintered samples showed crystallized hydroxyapatite (HA) while the pattern of non-sintered samples showed broader peaks indicating that the precipitate was an apatite (Fig. 1b). The crystal dimensions of the apatite were measured using ESEM (Fig. 1c), and the average crystal size was 84±19 nm width and 369±41 nm length, which confirmed the nano-dimensions of the material. ESEM also showed that the morphology of apatite crystals was needle-shaped (Fig. 1c).

Nano-apatite / poly(D,L-lactide) composites. The nano-apatite distribution was observed in the composites using back-scattered scanning electron microscopy. It was seen that the apatite crystals were homogeneously distributed throughout the composites (Fig. 2). The density of the composites increased proportionally with the apatite concentration (0% CaP: 1.13±0.34 g/ml; 10% CaP: 1.17±0.38 g/ml; 20% CaP: 1.22±0.36 g/ml; 40% CaP: 1.48±0.34 g/ml). FTIR showed an increase of the characteristic apatite peaks (around 560 cm^{-1} and 600 cm^{-1}) with the increase of apatite content in the materials and a decrease of the main polylactide peak around 1100 cm^{-1} (Fig. 3). At low magnification (25×), the blocks of all compositions (0% CaP, 10% CaP, 20% CaP and 40% CaP) had a similar porous structure, regardless of the apatite amounts (Fig. 4a, 4b, 4c, 4d) while at higher magnification (10,000×) they appeared to be slightly different due to the presence of apatite crystals, which created a more rough surface microstructure (Fig. 4e, 4f, 4g, 4h).

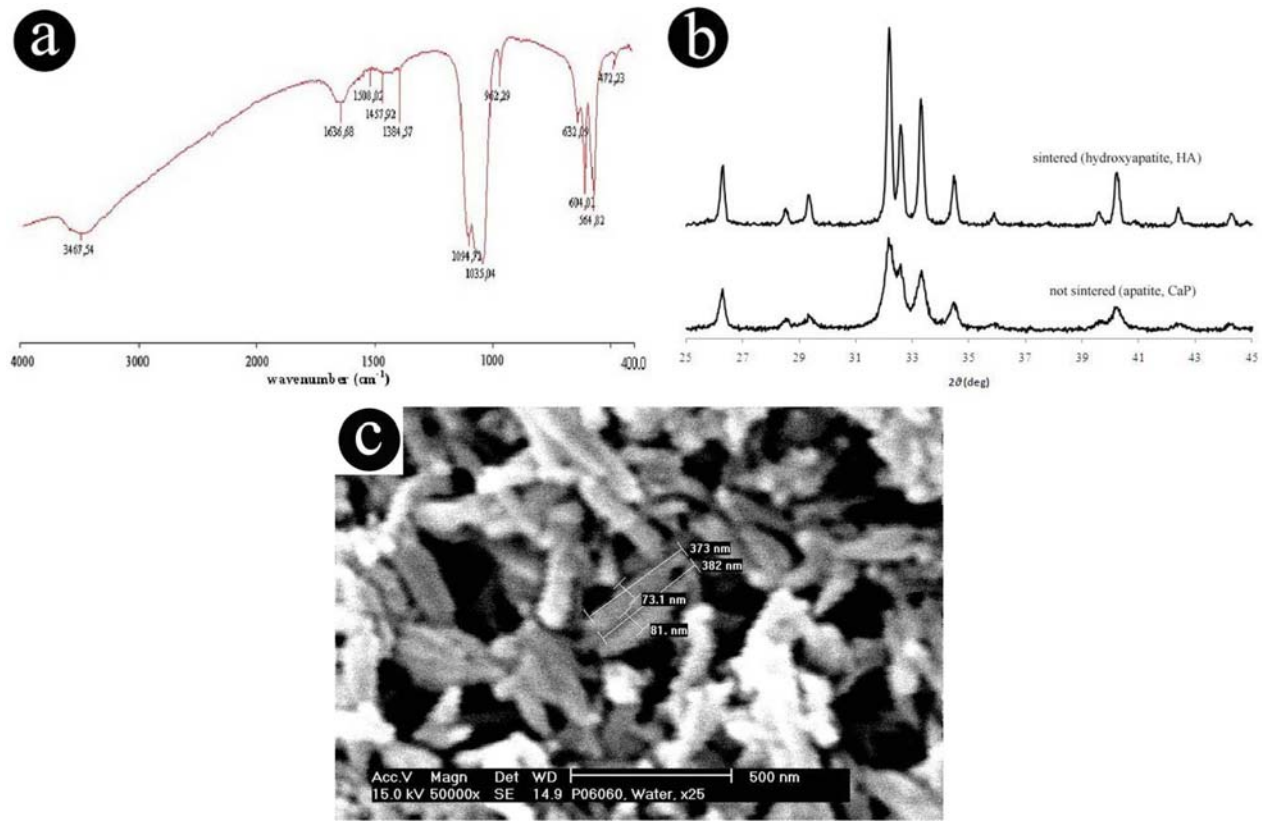

Fig. 1. (a) FTIR spectra of the not-sintered nano-apatite. **(b)** XRD spectra of the not-sintered nano-apatite (lower line) and of the sintered form (hydroxyapatite). **(c)** Measurements of the particle size of the not-sintered apatite were done using the ESEM.

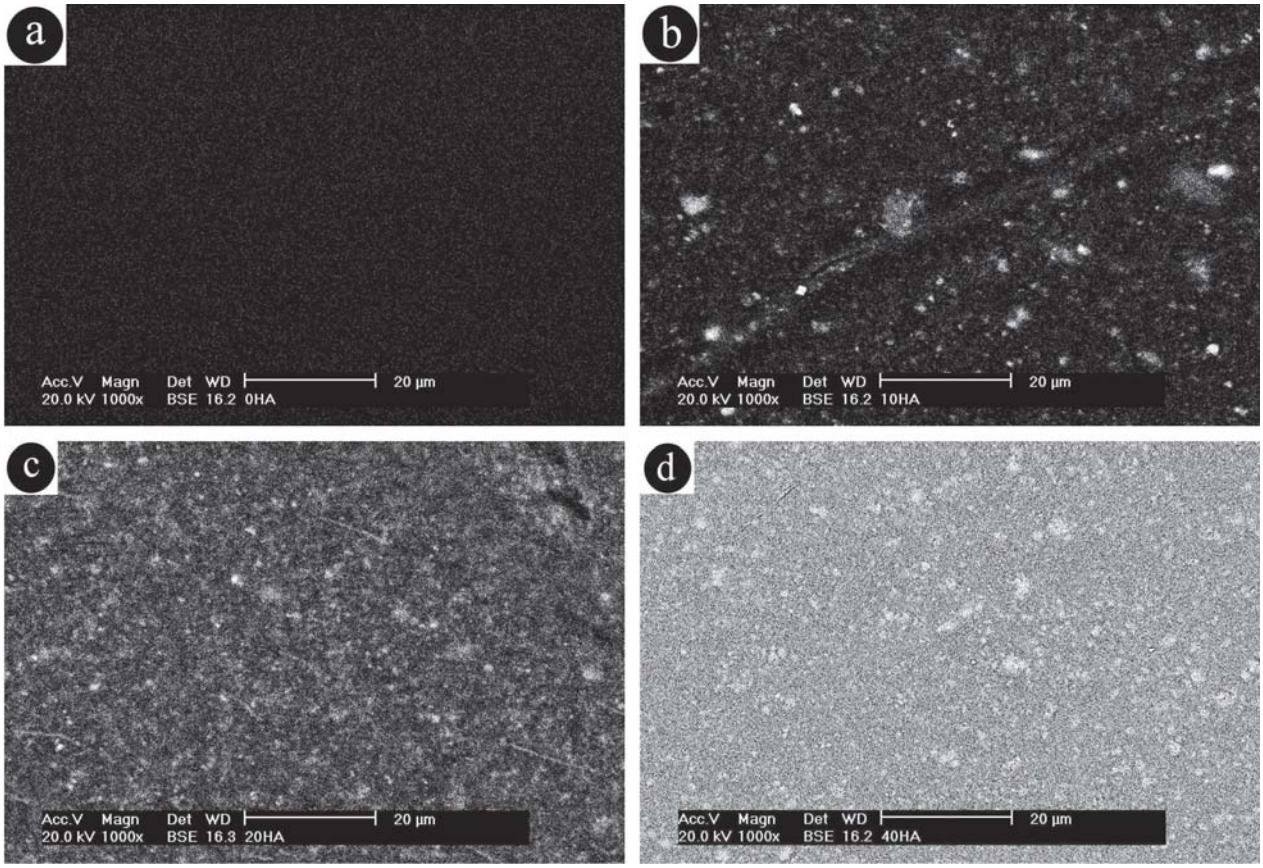

Figure 2. BSEM pictures showing the apatite particles distribution into the polylactide matrix. **(a)** 0% CaP (polylactide), **(b)** 10% CaP composite, **(c)** 20% CaP composite, **(d)** 40% CaP composite.

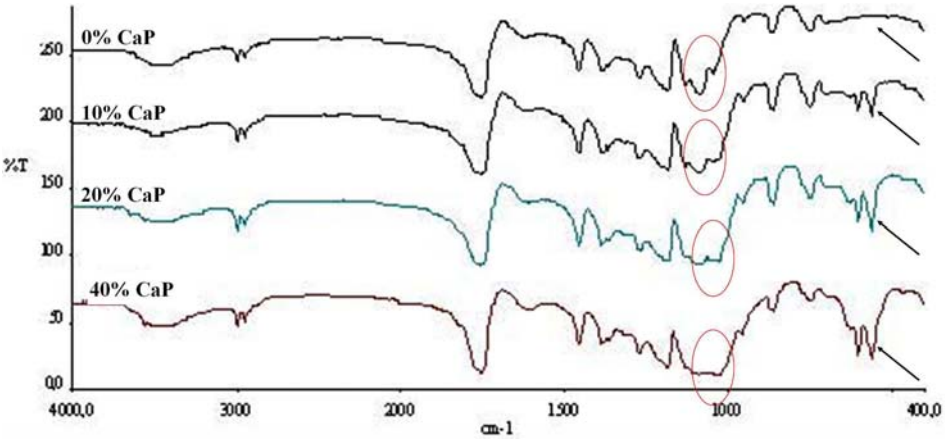

Fig. 3. FTIR spectra of the composites: it can be noticed that the apatite characteristic peaks depths increase with its amount within the composites (arrows) while one of the peaks of poly(D,L-lactide) disappears with the decrease of the polymer content (circles).

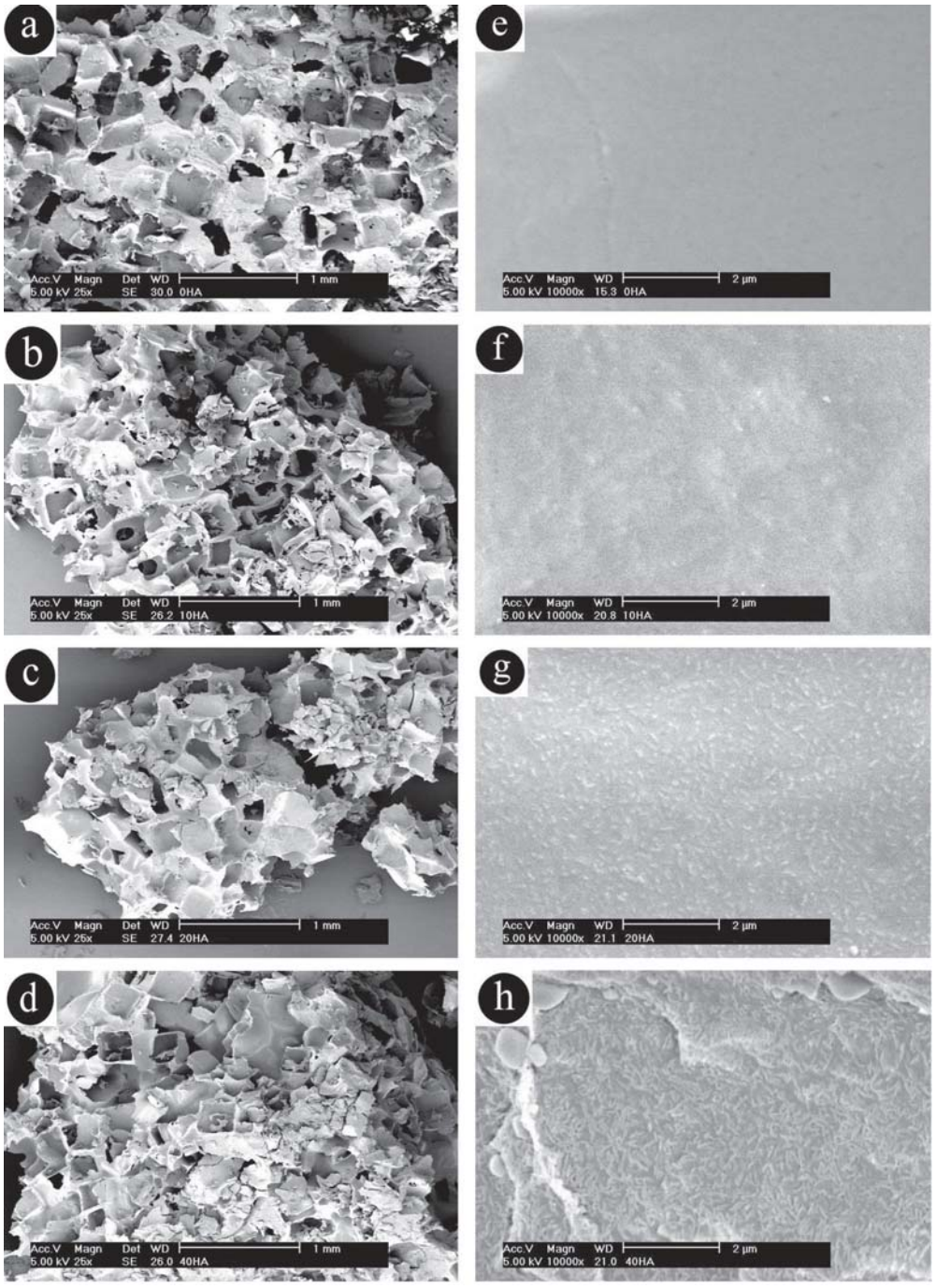

Fig. 4. ESEM pictures showing the porous sample of the composites at low (25×) and high (10,000×) magnifications. **(a)** 0% CaP sample. **(b)** 10% CaP sample. **(c)** 20% CaP sample. **(d)** 40% CaP sample. **(e)** Detail of the surface of 0% CaP sample. **(f)** Detail of the surface of 10% CaP sample. **(g)** Detail of the surface of 20% CaP sample. **(h)** Detail of the surface of 40% CaP sample.

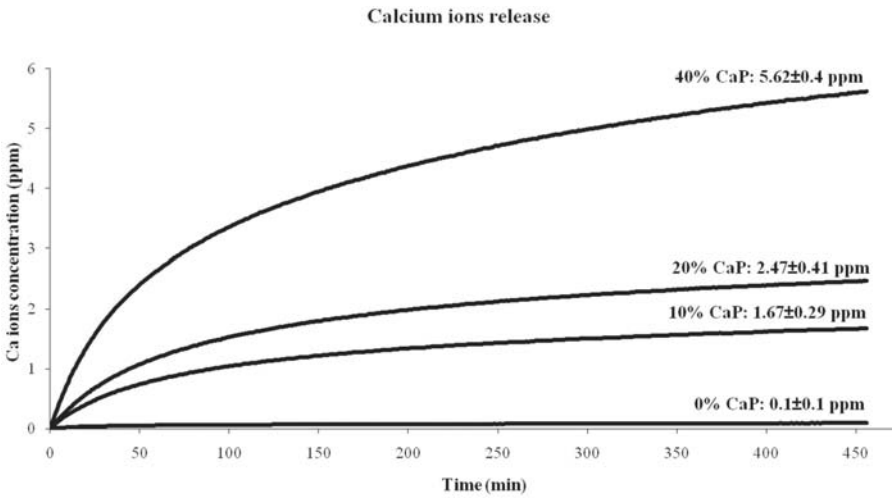

Fig. 5. Changes of calcium ions concentration in SPS when soaking the samples into SPS pH 7.3. The measurements were taken for 8 hours. On the diagram the final calcium ions concentrations in SPS are reported for each material.

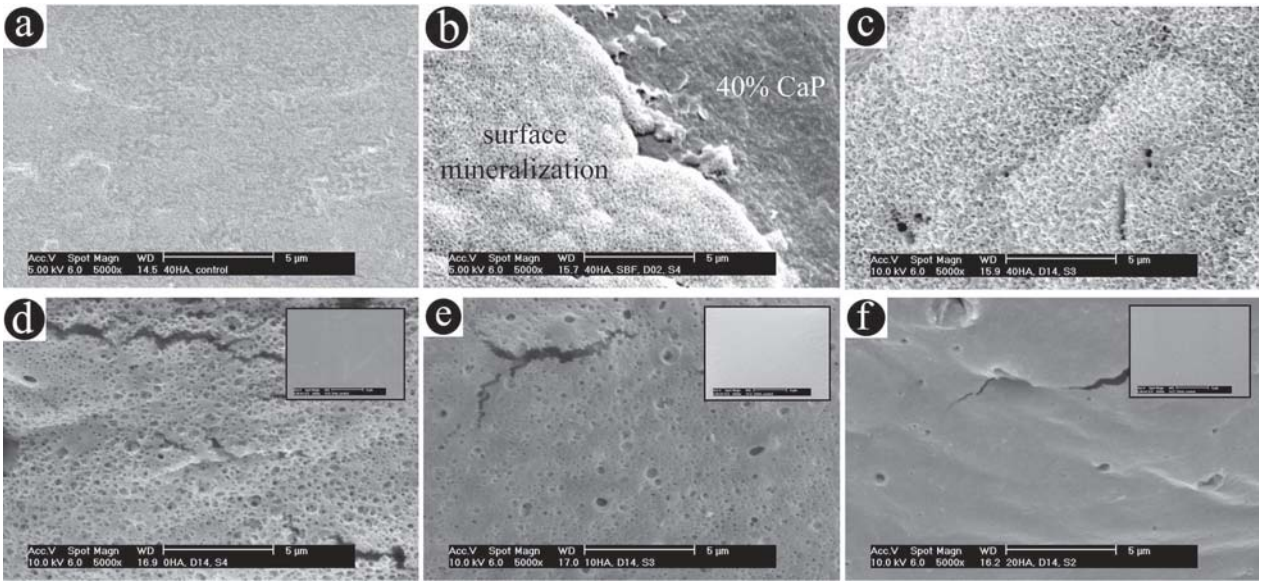

Fig. 6. Surface mineralization was seen after 2 days on 40% CaP, while it did not occur on the other composites after 2 weeks. **(a)** 40% CaP surface before soaking in SBF, **(b)** 40% CaP after 2 days soaking in SBF. It can be seen that surface mineralization is occurring on the 40% CaP samples. **(c)** 40% CaP after 14 days soaking in SBF. The samples surface is completely covered by a mineralized layer. **(d)** 0% CaP after 14 days soaking in SBF. In the small box the surface of 0% CaP before soaking in SBF. **(e)** 10% CaP after 14 days soaking in SBF. In the small box the surface of 10% CaP before soaking in SBF. **(f)** 20% CaP after 14 days soaking in SBF. In the small box the surface of 20% CaP before soaking in SBF.

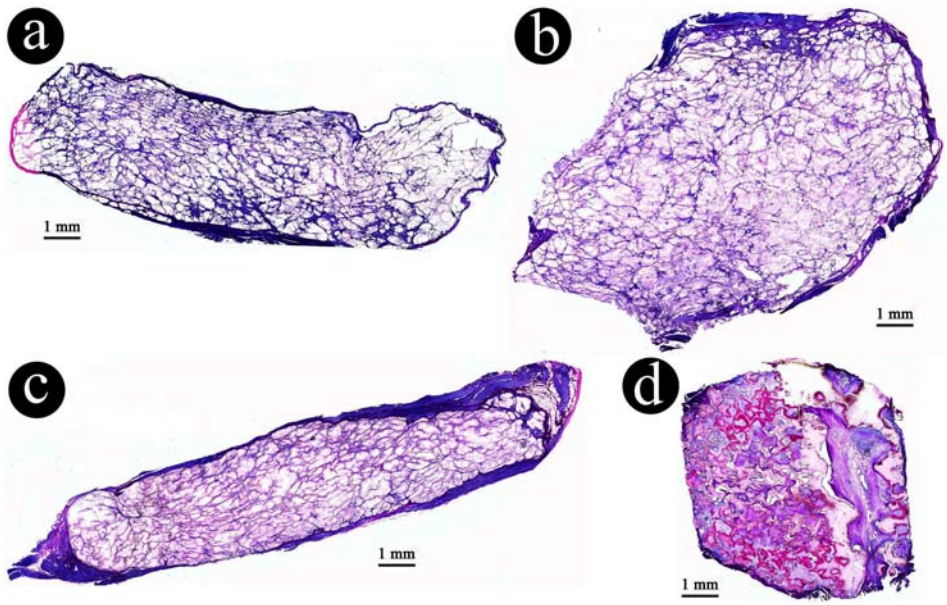

Fig. 7. Overview (with scanner) of stained sections (blue methylene-basic fuchsin staining) after 12 weeks implantation. **(a)** 0% CaP implant. **(b)** 10% CaP implant. **(c)** 20% CaP implant. **(d)** 40% CaP implant. It can be observed that bone formation occurred only in 40% CaP composites (d) while the porous structure of 0% CaP, 10% CaP and 20% CaP implants collapsed (a, b and c) as no porous architecture is anymore visible.

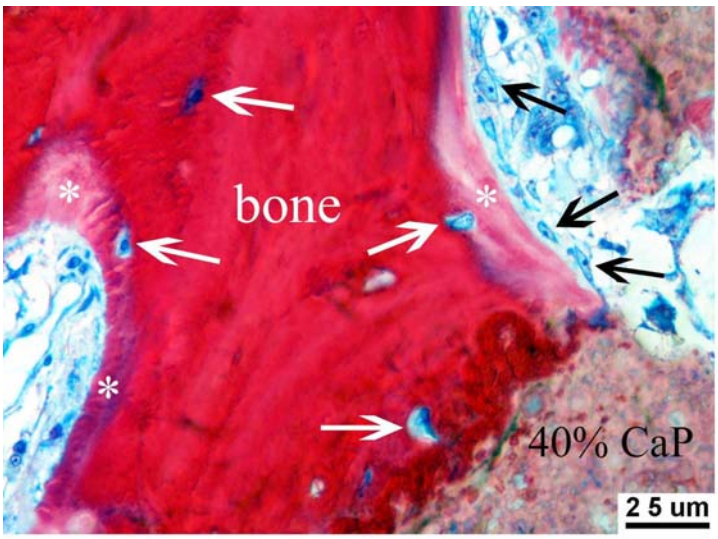

Fig. 8. Bone induction in 40% CaP after 12 weeks of intramuscular implantation. An active, but not yet mineralized, bone formation zone with a definite osteoblast-seam (black arrows) covering an osteoid layer (*) is visible. The inner part of the trabeculum is, as expected, an immature woven and mineralized bone with the typical large and polygonal osteocytes (white arrows).

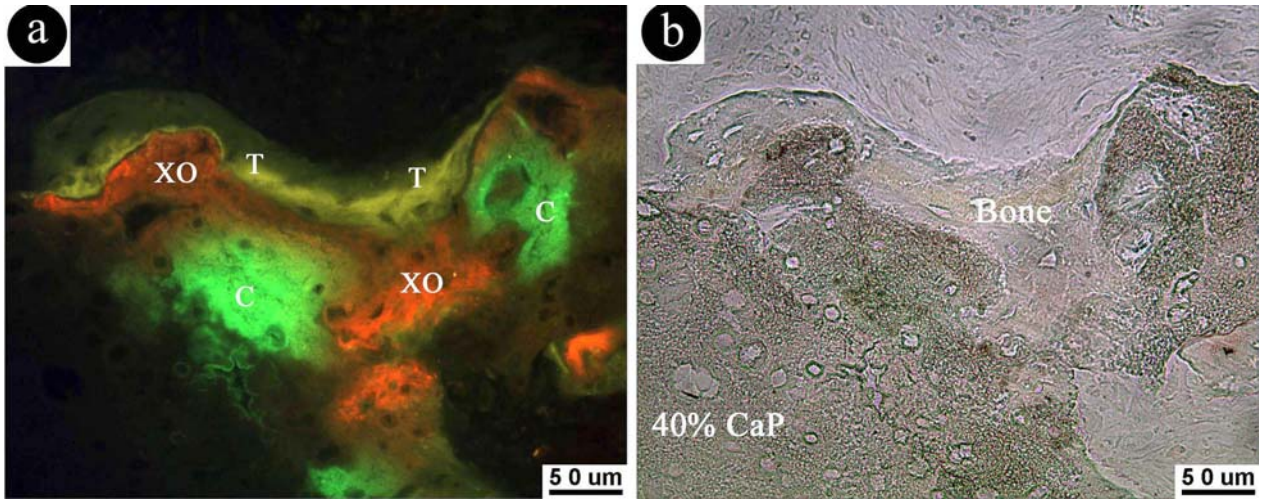

Fig. 9. By comparing micrographs of the same region of an unstained section under fluorescent **(a)** and transmitted light **(b)**, correlations between the composite (40% CaP) and the zone coloured in green (calcein, C, 3 wks), and between the bone formation (Bone) with the zones coloured in red (xylenol orange, XO, 6 wks) and yellow (tetracycline, T, 9 wks) are possible. This leads to the conclusion that bone started to form after 3 weeks but before 6 weeks from the implantation, while surface mineralization may have started to occur during the first 3 weeks.

In vitro calcium ion release

A correlation between calcium ion release and the amount of nano-apatite in the composites was observed (Fig. 5). Owing to the increase of calcium ion concentration into SPS, a decrease in the composite dissolution rate during time was seen for all samples. Moreover, the amount of calcium ions released was dependent on the apatite content in the material: the more apatite in the material, the faster the calcium ion release and the more ions released. After 8 hours, the calcium ions released from the materials were 5.62±0.4, 2.47±0.41, 1.67±0.29 and 0.1±0.1 ppm for 40% CaP, 20% CaP, 10% CaP and 0% CaP respectively.

In vitro surface mineralization

SEM images showed that the mineralization of the surface occurred *in vitro* after two days for all 40% CaP specimens (Fig. 6b), while for the materials with a lower apatite content no mineralization was seen within 14 days (Fig. 6d, 6e, 6f). The mineralization increased with time on the 40% CaP surface, as indicated by both the extension and the thickness of the covering calcified layer (Fig. 6a, 6b, 6c).

Ectopic bone formation

A total of 7 samples per material were intramuscularly implanted in 7 dogs. After 12 weeks, all samples were retrieved and they were surrounded by a thin layer of connective tissue and then muscle tissue. As shown in the histological overview (Fig. 7), only the 40% CaP specimens retained their shape after 12 weeks of implantation (Fig. 7d), while all samples with a lower CaP content had collapsed (Fig. 7a, 7b, 7c). It was also observed that only 40% CaP implants had *de novo* bone tissue in some pores (n=7) (Fig. 7d). Closer observation (Fig. 8) showed that both non-mineralized and mineralized bone had formed with no apparent gaps on the pore surface of all 40% CaP implants. Active osteoblast-like cells were present on the outer surface of the newly formed bone (Fig. 8), indicating that there was still active bone formation after 12 weeks of implantation. In the same time, osteocytes were observed within lacunae in the mineralized bone (Fig. 8). Histomorphometry showed that the area percentage of bone in the available space (i.e. in the pores) of 40% CaP was 4.9 ± 4.5% as determined with equation (1) (Table 1). Fluorescent microscopy showed that all 40% CaP

Table 1. Bone incidence, histomorphometrical data and fluorescent results after 12 weeks implantation in 7 dogs.

	0CaP	10CaP	20CaP	40CaP
number of implants	7	7	7	7
number of explants	7	7	7	7
bone incidence	0/7	0/7	0/7	7/7
bone formed in the pores (B_p%)	0 ± 0	0 ± 0	0 ± 0	4.9 ± 4.5
time for bone formation	no bone formation			between 3-6 wks

specimens contained the three colours: green, red and yellow (Fig. 9a). The colour green (calcein injected at week 3) was seen within the composite material and may indicate *in vivo* mineralization of the implants, and not bone formation. However, the presence of calcein in the material may also mean adsorption of the fluorochrome on the composite at free binding sites formed after degradation of the apatite. Red (xylenol orange injected at week 6) and yellow (tetracycline injected at week 9) fluorescent labels were seen within bone tissue deposited on the material surface and indicate that bone formation had started between 3 and 6 weeks (compare Fig. 9a and 9b) and had continued until at least 9 weeks after implantation. Table 1 summarizes the *in vivo* results.

Discussion

In the present study, we added nano-sized apatite into a polylactide matrix and obtained relatively homogenous composites with various apatite contents. All implants of 0% CaP, 10% CaP and 20% CaP had collapsed within 12 weeks *in vivo*, while 40% CaP retained its three-dimensional porous shape. Interestingly, the higher percentage of calcium phosphate apatite particles resulted in bone formation in the implants following intramuscular implantation. Since this phenomenon was shown in an ectopic implantation site, this can be defined as osteoinduction (Winter and Simpson, 1969). We have therefore shown that filling the polymer with high percentage of nano-scaled calcium phosphate apatite particles can render poly(D,L-lactide) osteoinductive. This property could be relevant when implanting these materials in large bone defects where osteoinduction is required (Kruyt *et al*., 2004; Habibovic *et al*, 2006a). The bone induction in 40% CaP started between 3 and 6 weeks after implantation, which is a time comparable to other osteoinductive materials such as biphasic calcium phosphate and hydroxyapatite, used in the same animal models (Yuan *et al*., 2006a).

At present it is not fully clear what triggers osteoinduction in the 40% CaP composites. Surface mineralization could play a role. In 1969 Winter and Simpson (Winter and Simpson, 1969) reported that a polymer induced bone formation under the skin of pigs and they observed that the surface of the polymer had mineralized before bone formation. Fujibayashi (Fujibayashi *et al*., 2004) also suggested a role of *in vitro* surface mineralization in material-directed bone induction. They compared the *in vivo* osteoinductivity (in muscle of dogs) of titanium implants, with surfaces that did or did not mineralize *in vitro* in SBF. Their results showed that titanium implants capable of forming an apatite layer in SBF also induced bone formation *in vivo*. Conversely, implants that did not mineralize *in vitro* also did not induce bone formation. We showed a similar relation between *in vitro* surface mineralization and bone induction using our composites. From the composites that were tested *in vitro* in SBF, only the surface of 40% CaP composites mineralized within 14 days. It is well-known that apatite-based materials contain functional groups that allow spontaneous formation of a mineralized layer onto their surfaces (Kokubo *et al*., 2000). Together with the high surface exposure of apatite in 40% CaP, this would explain the large and fast mineralization onto the 40% CaP composites. This result was similar to Shikinami and Okuno, who found that micron-sized hydroxyapatite/poly(L-lactide) composites rapidly formed (within one week) a mineralized layer onto their surfaces when immersed in SBF (Shikinami and Okuno, 1999). Similar to the observation of Winter and Simpson, 40% CaP may have mineralized *in vivo* before bone formation had occurred after 3 weeks of implantation (Fig. 9a, 9b). We therefore hypothesise that the nano-sized apatite enhanced surface mineralization of the 40% CaP composites *in vivo*, and therefore allowed bone induction *in vivo*. This is in line with the suggestion that *in vivo* surface mineralization generates a suitable environment for inducible cells to form bone (de Bruijn *et al*, 2008) and allows osteoinduction to occur (LeGeros, 2002; Kokubo *et al*., 2003). Besides *in vivo* surface mineralization, protein adsorption may also play a role in inducing ectopic bone formation in 40% CaP implants. It has been reported that a bioinert Al_2O_3 ceramic adsorbs proteins and induces bone formation in muscle of dogs while it was not shown to surface calcify *in vitro* or *in vivo* (Yuan *et al*., 2006b). It has also been shown that calcium phosphate materials have high affinity for proteins (e.g. bone morphogenetic proteins, BMPs) (LeGeros, 2002; Habibovic *et al*., 2005) and that composites with a high content of HA adsorb more proteins (Wei and Ma, 2004). Based on these assumptions, it may be hypothesized that the 40% CaP composites adsorb a high amount of proteins (including BMPs) from the surrounding body fluids and then trigger inductive bone formation. Conversely, composites with lower apatite content would not adsorb enough proteins to start inductive bone formation. The proteins that adsorb and play a potential role in 40% CaP osteoinduction needs to be evaluated in further studies.

Another aspect regarding inductive bone formation in 40% CaP may be ion release (especially calcium) from the composites. Calcium is an extra-cellular signalling molecule in bone (Yuan *et al*., 1998; Ducheyne and Qiu, 1999; Ripamonti *et al*., 1999; Habibovic *et al*., 2005) and it has been shown that ions released from calcium phosphate materials do not only enhance the bioactivity of materials (Daculsi *et al*., 1990; Ripamonti *et al*., 1999; Habibovic *et al*., 2005) but also the proliferation, differentiation and mineralization of osteogenic cells (Ducheyne and Qiu, 1999). We found a higher amount of calcium ions released *in vitro* from 40% CaP composites

compared to the others and, as shown in this study, only 40% CaP gave rise to inductive bone formation, indicating a possible effect of the amount of calcium ion released on the osteoinduction. The higher release of calcium ions from 40% CaP, as compared to the other three considered materials, might be due to the fact that 40% CaP composite exposes more apatite on its surface. After degradation, the released calcium may have enhanced osteoinduction (Zaffe, 2005).

Finally, the surface microstructural changes due to the increased apatite content in the four composites could have played a role in bone induction. Several studies have reported that controlled micro- or nano-structures do not only have positive effects on the differentiation of mesenchymal stem cells into osteogenic cells (Dalby *et al*., 2007), but also influence protein adsorption and ion release (Habibovic *et al*., 2005, de Bruijn *et al*., 2008; Zhu *et al*., 2009). As shown in Figures 4e, 4f, 4g and 4h, the 40% CaP has a rougher surface microstructure as compared to composites with lower apatite contents. Previous studies have shown that a specific surface microstructure on a chemically unaltered ceramic can render osteoinductive ceramics (Yuan *et al*., 1999; Habibovic *et al*., 2005; de Bruijn *et al*., 2008). We have also shown that porous tantalum, coated with a biomimetic octacalcium phosphate coating, is osteoinductive when implanted in the muscle of dogs (de Bruijn *et al*., 2000). The observed change in surface microstructure with 40% CaP by exposed nano-apatite particles could have been further enhanced during resorption of the polymer phase.

Implants having less than 40% CaP collapsed and no bone formation occurred. Although the lack of a porous architecture may have inhibited bone formation (Yuan *et al*., 1998; Kurashina *et al*., 2002; Habibovic *et al*., 2005), we have recently shown that macroporosity of a scaffold is not a prerequisite for bone induction to occur (de Bruijn *et al*., 2008). This suggests that the absence of bone formation in composites with lower contents of CaP apatite is due to the apatite content and not the lack of a porous architecture.

The current results cannot conclusively assign inductive bone formation in 40% CaP to surface mineralization, protein adsorption, calcium ion release and/or surface microstructure. It may well be that these features played a combined role in the observed osteoinduction by the 40% CaP composite. Nonetheless, the influence of nano-sized calcium phosphate apatite particles in inductive bone formation has clearly been shown. It provides a microstructured surface morphology and enhances surface mineralization, ion release and protein adsorption eventually resulting in heterotopic ossification of high apatite content composites.

Conclusion

In the quest to develop the ideal bone graft material, we have prepared an osteoinductive composite based on poly(D,L-lactide) and nano-sized apatite. The influence of nano apatite on the osteoinductive properties of the composites was shown. Forty weight percent nano-apatite provided a structural composite with a microstructured surface, enhancing ion release and surface mineralization, which ultimately led to ectopic bone formation in the dorsal muscle of dogs. Future studies will focus on enhancing mechanical properties and understanding the process of material directed osteoinduction.

Acknowledgments

The authors gratefully acknowledge the support of the Smart Mix Program of the Netherlands Ministry of Economic Affairs and the Netherlands Ministry of Education, Culture and Science. The authors also would like to thank Dr. Chongyun Bao (Sichuan University, Chengdu, China) for the assistance with the animal studies in China.

References

Daculsi G, LeGeros RZ, Heughebaert M, Barbieux I (1990) Formation of carbonate-apatite crystals after implantation of calcium phosphate ceramics. Calcif Tissue Int **46**: 20-27.

Dalby MJ, Gadegaard N, Tare R, Andar A, Riehle MO, Herzyk P, Wilkinson CD, Oreffo RO (2007) The control of human mesenchymal cell differentiation using nanoscale symmetry and disorder. Nat Mater **6**: 997-1003.

Deng X, Hao J, Wang C (2001) Preparation and mechanical properties of nanocomposites of poly(D,L-lactide) with Ca-deficient hydroxyapatite nanocrystals. Biomaterials **22**: 2867-2873.

de Bruijn JD, Yuan H, Dekker R, Layrolle P, de Groot K, van Blitterswijk CA (2000) Osteoinductive biomimetic calcium-phosphate coatings and their potential use as tissue-engineering scaffolds. In: Bone Engineering (JE Davies, ed), EM Square Inc, Toronto, pp 421-431.

de Bruijn JD, Shankar K, Yuan H, Habibovic P (2008) Osteoinduction and its evaluation. In: Bioceramics and their Clinical Applications (T Kokubo, ed), Woodhead Publishing, CRC Press, Boca Raton, FL, pp 199-219.

Ducheyne P, Qiu Q (1999). Bioactive ceramics: the effect of surface reactivity on bone formation and bone cell function. Biomaterials **20**: 2287-2303.

Fellah BH, Gauthier O, Weiss P, Chappard D, Layrolle P (2008) Osteogenicity of biphasic calcium phosphate ceramics and bone autograft in a goat model. Biomaterials **29**: 1177-1188.

Fujibayashi S, Neo M, Kim HM, Kokubo T, Nakamura T (2004) Osteoinduction of porous bioactive titanium metal. Biomaterials **25**: 443-450.

Giannoudis PV, Dinopoulos H, Tsiridis E (2005) Bone substitutes: an update. Injury **36**: s20-s27.

Habibovic P, Yuan H, van der Valk CM, Meijer G, van Blitterwijk CA, de Groot K (2005) 3D microenvironment as essential element for osteoinduction by biomaterials. Biomaterials **26**: 3565-3575.

Habibovic P, Yuan H, van den Doel M, Sees TM, van Blitterswijk CA, de Groot K (2006a) Relevance of osteoinductive biomaterials in critical-sized orthotopic defect. J Orthop Res **24**: 867-876.

Habibovic P, Sees TM, van den Doel MA, van Blitterswijk CA, de Groot K (2006b) Osteoinduction by

biomaterials – physicochemical and structural influences. J Biomed Mater Res **77A**: 747-762.

Hollinger JO, Brekke J, Gruskin E, Lee D (1996) Role of bone substitute Clin Orthop **324**: 55-66.

LeGeros RZ (2002) Properties of osteoconductive biomaterials: calcium phosphates. Clin Orthop Relat Res **395**: 81-98.

Kokubo T, Kim HM, Kawashita M, Nakamura T (2000) What kinds of materials exhibit bone-bonding? In: Bone Engineering (JE Davies, ed), EM Square Inc, Toronto, pp 190-194.

Kokubo T, Kim HM, Kawashita M (2003) Novel bioactive materials with different mechanical properties. Biomaterials **24**: 2161-2175.

Kokubo T, Takadama H (2006) Leading opinion. How useful is SBF in predicting *in vivo* bone bioactivity? Biomaterials **27**: 2907-2915.

Kondo N, Ogose A, Tokunaga K, Umezu H, Arai K, Kudo N, Hoshino M, Inoue H, Irie H, Kuroda K, Mera H, Endo N (2006) Osteoinduction with highly purified beta-tricalcium phosphate in dog dorsal muscles and the proliferation of osteoclasts before heterotopic bone formation. Biomaterials **27**: 4419-4427.

Kruyt MC, Dhert WJ, Yuan H, Wilson CE, van Blitterwijk CA, Verbout AJ, de Bruijn JD (2004) Bone tissue engineering in a critical size defect compared to ectopic implantations in the goat. J Orthop Res **22**: 544-551.

Kurashina K, Kurita H, Wu Q, Ohtsuka A, Kobayashi H (2002) Ectopic osteogenesis with biphasic ceramics of hydroxyapatite and tricalcium phosphate in rabbits. Biomaterials **23**:407-412.

Le Nihouannen D, Daculsi G, Saffarzadeh A, Gauthier O, Delplace S, Pilet P, Layrolle P (2005) Ectopic bone formation by microporous calcium phosphate ceramic particles in sheep muscles. Bone **36**: 1086-1093.

Lin PL, Fang HW, Tseng T, Lee WH (2007) Effects of hydroxyapatite dosage on mechanical and biological behaviors of polylactic acid composite materials. Mat Lett. **61**: 3009-3013.

Navarro M, Michiardi A, Castaño O, Planell JA (2008) Biomaterials in orthopaedics. J R Soc Interface **5**: 1137-1158.

Nejati E, Mirzadeh H, Zandi M (2008) Synthesis and characterization of nano-hydroxyapatite rods/poly(L-lactide acid) composite scaffold for bone tissue engineering. Composites Part A **39**: 1589-1596.

Rezwan K, Chen QZ, Blaker JJ, Boccaccini AR (2006) Review. Biodegradable and bioactive porous polymer/inorganic composite scaffolds for bone tissue engineering. Biomaterials **27**: 3413-3431.

Ripamonti U (1996) Osteoinduction in porous hydroxyapatite implanted in heterotopic sites of different animal models. Biomaterials **17**: 31-35.

Ripamonti U, Crooks J, Kirkbride AN (1999). Sintered porous hydroxyapatites with intrinsic osteoinductive activity: geometric induction of bone formation. S Afr J Sci **95**: 335-43.

Rodríguez-Lorenzo LM, Vallet-Regí M (2000) Controlled crystallization of calcium phosphate apatites. Chem Mater **12**: 2460-2465.

Shikinami Y, Okuno M (1999) Bioresorbable devices made of forged composites of hydroxyapatite (HA) particles and poly-L-lactide (PLLA): Part I. Basic characteristics. Biomaterials **20**: 859-877.

Verheyen CC, de Wijn JR, van Blitterswijk CA, de Groot K, Rozing PM (1993) Hydroxylapatite / poly(L-lactide) composites: an animal study on push-out strengths and interface histology. J Biomed Mater Res **27**: 433-444.

Wei G, Ma PX (2004) Structure and properties of nano-hydroxyapatite/polymer composite scaffolds for bone tissue engineering. Biomaterials **25**: 4749-4757.

Winter GD, Simpson BJ (1969) Heterotopic bone formation in a synthetic sponge in the skin of young pigs. Nature **223:** 88-90.

Yamasaki H (1990) Heterotopic bone formation around porous hydroxyapatite ceramics in the subcutis of dogs. Jpn J Oral Biol **32**:190-192.

Yuan H, Yang Z, Li Y, Zhang X, de Bruijn JD, de Groot K (1998) Osteoinduction by calcium phosphate biomaterials. J Mater Sci: Mater Med **9**: 723-726.

Yuan H, Kurashina K, de Bruijn JD, Li Y, de Groot K, Zhang X (1999) A preliminary study on osteoinduction of two kinds of calcium phosphate ceramics. Biomaterials **20**: 1799-1806.

Yuan H, van Blitterswijk CA, de Groot K, de Bruijn JD (2006a) A comparison of bone formation in biphasic calcium phosphate (BCP) and hydroxyapatite (HA) implanted in muscle and bone of dogs at different time periods. J Biomed Mater Res A **78**: 139-147.

Yuan H, van Blitterswijk CA, de Groot K, de Bruijn JD (2006b) Ectopic bone formation by microstructured synthetic materials through *in vivo* protein adsorption. Trans 31st Ann Meet Soc Biomaterials, Vol XXIX, p 609.

Zaffe D (2005) Some considerations on biomaterials and bone. Micron **36**: 583-592.

Zhu XD, Fan HS, Xiao YM, Li DX, Zhang HJ, Luxbacher T, Zhang XD (2009) Effect of surface structure on protein adsorption to biphasic calcium-phosphate ceramics *in vitro* and *in vivo*. Acta Biomaterialia **5**:1311-1318.

Discussion with Reviewer

R.G. Richards: This increased Ca-concentration in the SBF could be the major cause for surface mineral deposition by precipitation. Please comment.

Authors: The amount of calcium released *in vitro* in SPS over 8 hours is very limited (0.14 mM) as compared to the starting calcium concentration in SBF (2.5 mM) where we observed possible degradation of materials. As we suppose that the calcium release in SBF may be about the same amount recorded in SPS, the small increase in calcium concentration in SBF due to the release of calcium cannot be enough for being the trigger for the mineralization.